

## AN INTEGRODIFFERENTIAL MODEL FOR ORIENTATIONAL DISTRIBUTIONS OF F-ACTIN IN CELLS\*

EDITH GEIGANT<sup>†</sup>, KARINA LADIZHANSKY<sup>‡</sup>, AND ALEXANDER MOGILNER<sup>§</sup>

**Abstract.** Angular self-organization of the actin cytoskeleton is modeled as a process of instant changing of filament orientation in the course of specific actin-actin interactions. These interactions are modified by cross-linking actin-binding proteins. This problem was raised first by Civelekoglu and Edelstein-Keshet [*Bull. Math. Biol.*, 56 (1994), pp. 587–616]. When restricted to a two-dimensional configuration, the mathematical model consists of a single Boltzmann-like integrodifferential equation for the one-dimensional angular distribution. Linear stability analysis, asymptotic analysis, and numerical results reveal that at certain parameter values of actin-actin interactions, spontaneous alignment of filaments in the form of unipolar or bipolar bundles or orthogonal networks can be expected.

**Key words.** actin cytoskeleton, master equation, Boltzmann equation, integrodifferential equation, peak solution

**AMS subject classifications.** 45K05, 92C

**PII.** S0036139996309539

**1. Introduction.** The formation of orientational order has been of great scientific interest during the last several years. Fish schools and flocks of birds are characterized by a high degree of directionality. Various models were suggested to explain the parallel alignment of bacteria in swarms [15] and the formation of parallel arrays of fibroblasts [4]. Here we are interested in orientational patterns on a molecular biological level.

Actin is an abundant protein in cells. It is the main building material for the cytoskeleton, playing an important role in intracellular transport, cell motility, and division [16], [18], [20], [7], [22]. We will concentrate on the properties of actin in nonmuscle cells. Actin exists in these cells in a variety of types of structural order, ranging from disordered loose meshworks to highly ordered fibers and bundles. Actin filaments consist of monomers (*G*-actin) that, to first approximation, are polymerized in linear order. The length of the filament can change very rapidly. Monomers usually are attached at, and leave the filament from, the ends of the polymer. There is no symmetry between the “head” and the “tail” of an actin polymer because monomers are not isotropic and bind each other in a geometrically ordered manner.

For our purposes a model of an individual actin filament as a rigid rod will do.

---

\*Received by the editors September 20, 1996; accepted for publication (in revised form) July 24, 1997; published electronically December 11, 1998. This work was supported by NATO International Scientific Exchange Programme Collaborative Research grant 931073 to Profs. W. Alt and L. Edelstein-Keshet, NSERC operating grant OGPIN 021 to Prof. L. Edelstein-Keshet, UGF (University of British Columbia), and by a fellowship from the Program in Mathematics and Molecular Biology at the University of California at Berkeley, which is supported by the NSF under grant DMS-9406348.

<http://www.siam.org/journals/siap/59-3/30953.html>

<sup>†</sup>Department of Theoretical Biology, Universität Bonn, Kirschallee 1, D-53115 Bonn, Germany (edith.geigant@uni-bonn.de). The work of this author was supported by a doctorate grant of the Studienstiftung des deutschen Volkes.

<sup>‡</sup>Department of Applied Mathematics and Computer Science, Weizmann Institute of Science, Rehovot 76100, Israel (yusim@wisdom.weizmann.ac.il).

<sup>§</sup>Department of Mathematics, University of California, Davis, CA 95616 (mogilner@ucdmath.ucdavis.edu).

It was shown in a number of experiments that our assumption is justified if filaments are short, if the time interval during which stress is applied is short, or if the applied stress is weak [9]. More precisely, filaments of length  $0.1 - 1\mu m$  (80–90% of filaments *in vivo* are of this length) are stiff. Even longer filaments associated with certain proteins (e.g., tropomyosin) or heavily cross-linked can be viewed as straight rods.

The spatioangular organization of actin in the cytoskeleton is vitally important for the life of the cell, and this organization has to be changed rapidly when needed. This is achieved and controlled with the help of an extensive variety of actin-binding proteins, such as  $\alpha$ -actinin, filamin, fibrillin, ABP-280, and myosin—to name just a few. In this paper we completely ignore the army of proteins binding actin to the cell membrane, severing it, etc., concentrating instead on the actin-binding proteins that provide short- or long-living links between neighboring filaments.

The spatial structure of the cytoskeleton leads to important effects in cell biology [18] and promises interesting mathematical modeling [13]. Nevertheless, in the present paper we do not attempt to model the spatial structure of the cytoskeleton, considering it to be spatially homogeneous. This is a sensible approach if we work with a small volume in the cell that contains a large number of actin filaments. It is the angular order of actin that is the object of our investigation here.

Static mechanical properties of the cell depend on the angular structure of the actin network [7]. Also, in lamellipodia of some cells, bulk retrograde flow of actin (which is an important component of motility) driven by myosin depends critically on the orientation of actin fibers [3]. A few types of angular order have been detected and are known to be important [16], [18], [20], [7], [22]:

1. completely loose gel-like isotropic actin meshworks;
2. more structured anisotropic meshworks where micrographs reveal that most angles between the filaments are close to the right angle (orthogonal meshworks); and
3. bundles, where actin is aligned along some axis, prescribed by external conditions. Bundles may be
  - (i) unipolar (all heads are oriented in the same direction) or
  - (ii) bipolar (heads are aligned along two opposite directions).

*In vivo*, these structures are usually three-dimensional (with some important exceptions, such as two-dimensional orthogonal actin networks at the lamellipodia of keratocytes [18]). *In vitro*, similar two-dimensional structures are observed [21]. In the present model we attempt to explain these types of order.

An important difference between angular self-ordering in liquid crystals and that in the cytoskeleton is that the former is partially due to crowding effect. Simple estimates show that the cytoskeleton *in vivo*, when the mesh size is about  $0.1\mu m$ , is far from being crowded, so this factor is less important than protein-mediated actin-actin interaction. In this case, modeling approaches employing nonlinear phenomenological equations governing the angular and temporal dynamics of average densities might be appropriate.

The angular organization of the cytoskeleton was modeled lately using various ideas [2], [10], [17]. A phenomenological functional of the actin angular distribution dependent on mechanical forces was introduced by Sherratt and Lewis [17]. Minimization of this functional gave a resulting angular ordering. Madden and Herzfeld [10] analyzed a free energy of a crowded ensemble of growing and depolymerizing actin fibers. Also, the alignment was obtained by minimization of a free-energy functional. These models imply that the system is close to thermodynamic equilibrium. However, the cytoskeleton of the living cell is far away from such equilibrium [20]. Moreover,

one of the advantages of a dynamical approach is that it allows one to analyze the system's approach to a stationary state.

Such a dynamical model was suggested earlier in [4] and applied to the cytoskeleton dynamics in [2]. This is a model describing the dynamics of two two-dimensional angular densities—that of “bound” actin and that of “free” actin—with a complex set of integrodifferential equations. The mathematical analysis of these papers was extended in [11], [12]. The present paper is related to the work of Civelekoglu and Edelstein-Keshet [2] and uses the same general approach. However, the following reasons forced us to suggest another model. For the dense actin meshwork, it is, in general, difficult to distinguish between “bound” and “free” types of filaments, and also free rotational diffusion of the fibers (which was the antiordering factor in [2]) is unimportant.

The following scenario leads to the mathematical model described in the next section. The model assumes the existence of groups of actin filaments in the cytoplasm attached to some hypothetical “nods” (see also [1]). Within each group the fibers are cross-linked with actin-binding proteins. In cells the actin-related interaction mechanisms are diverse and complex. However, mechanistic interaction rules can be formulated and put into an appropriate mathematical framework. These rules are based on the properties of different actin-binding proteins which have different binding affinities and configurations and which favor different orientational structures. Actin-binding proteins are viewed as being able to bind two filaments together. The rates of attachment and detachment are angle and density dependent. Frequent detachment of a filament from proteins and attachment to another protein redistribute the filament.

We consider various mechanisms of alignment by actin-binding proteins, partly based on experimental data and partly on speculations. Some proteins, like gelsolin, are very long and, hence, flexible rods. Two filaments linked by such proteins are, on the average, oriented with an angular uncertainty so great that they reveal little or no alignment. The protein  $\alpha$ -actinin is a shorter rod. Filaments linked by it align with each other with less uncertainty and create loose bundles. The protein fibrillin is very stiff and favors tight bundles. Myosin II has two tails “glued” together and two heads. The heads attach to actin in a sterically precise way and align them in a bipolar fashion (with “heads” of the two fibers oriented opposite to each other). Filamin is abundant in orthogonal meshworks. This protein may work as a specific floppy hinge with two “arms” perpendicular to each other. Two filaments attaching to different arms of filamin will be at right angles to each other.

This picture leads to the following model. Each actin filament is described by its orientational angle  $\theta \in (-\pi, \pi]$ . (Here we restrict ourselves to the two-dimensional model.) As a result of detachment and turning, filaments disappear from direction  $\theta$  with a certain rate. At the same time, as a result of actin-actin interaction, other fibers from other directions appear at direction  $\theta$ . This leads to a discontinuous description of the angular dynamics with a nonlinear integrodifferential Boltzmann-like master equation. We call the corresponding angle-dependent rate a turning probability function. There are no experimental data on such rates, mainly because it has been impossible so far to observe individual fibers *in vivo*. We speculate on the angular dependence of this rate based on available structural information about actin-binding proteins. Also, earlier modeling [11], as well as this paper, demonstrates that the type of order mainly depends on the symmetry properties of the interactions rather than on the detailed angular dependence of the corresponding rates.

The paper is organized as follows. We introduce the mathematical model in

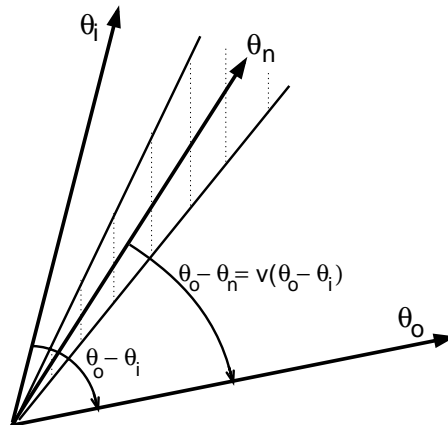


FIG. 1. Sketch of filaments and mutual angles. With high probability the filament's turning angle is near an "optimal" turning angle,  $\theta_o - \theta_n = v(\theta_o - \theta_i)$ . After turning, the new position of filament  $\theta_o$  will most probably be in the shaded area.

section 2. Section 3 is devoted to a linear stability analysis of the model. A limiting case of complete alignment in one direction is investigated in section 4. We report results of numerical simulations in section 5. The discussion in section 6 concludes the paper.

## 2. The mathematical model.

**2.1. Definitions and master equation.** Throughout this paper we use the following notations:

$t$	time, $t \geq 0$ ,
$\theta$	orientation angle, $\theta \in (-\pi, \pi]$ ,
$f(\theta, t)$	angular distribution of filaments,
$\eta(\theta_o - \theta_i)$	rate (per unit time) of interaction between two filaments at directions $\theta_o, \theta_i$ ,
$w(\theta_o - \theta_n, \theta_o - \theta_i)$	probability of turning of a filament from direction $\theta_o$ to direction $\theta_n$ as a result of interactions with filaments at direction $\theta_i$ ; see Figure 1.

All functions are  $2\pi$ -periodic (in all variables).

The ensemble of fibers is characterized by the angular distribution  $f(\theta, t)$ . A filament turns effectively in the course of a pairwise interaction with another filament, mediated by actin-binding proteins. We consider the isotropic case characterized by local rotational invariance of the cytoplasm. Thus, all relevant elementary rates and probabilities depend on the relative angles only, not on angles measured from some distinguished axis. We call the functions  $w(\theta_o - \theta_n, \theta_o - \theta_i)$  and  $\eta(\theta_o - \theta_i)$  *turning probability function* and *frequency function*, respectively. Since  $w$  is a probability density,

$$(2.1) \quad \int_{-\pi}^{\pi} w(\theta_o - \theta_n, \theta_o - \theta_i) d\theta_n = 1.$$

Rescaling the time yields

$$(2.2) \quad \int_{-\pi}^{\pi} \eta(\theta_o - \theta_i) d\theta_i = 1.$$

Thus, the rate of turning from angle  $\theta_o$  to angle  $\theta_n$  is a linear functional of  $f$ :

$$(2.3) \quad W[f](\theta_o, \theta_n) = \int_{-\pi}^{\pi} \eta(\theta_o - \theta_i) w(\theta_o - \theta_n, \theta_o - \theta_i) f(\theta_i) d\theta_i.$$

The following master equation governs the dynamics of the angular distribution [14]:

$$(2.4) \quad \frac{\partial f}{\partial t}(\theta, t) = -f(\theta, t) \int_{-\pi}^{\pi} W[f](\theta, \theta_n) d\theta_n + \int_{-\pi}^{\pi} W[f](\theta_o, \theta) f(\theta_o, t) d\theta_o,$$

or, plugging in expression (2.3) for the rate  $W$  and taking into account condition (2.1),

$$(2.5) \quad \begin{aligned} \frac{\partial f}{\partial t}(\theta, t) = & -f(\theta, t) \int_{-\pi}^{\pi} \eta(\theta - \theta_i) f(\theta_i, t) d\theta_i \\ & + \int_{-\pi}^{\pi} \int_{-\pi}^{\pi} w(\theta_o - \theta, \theta_o - \theta_i) \eta(\theta_o - \theta_i) f(\theta_o, t) f(\theta_i, t) d\theta_i d\theta_o. \end{aligned}$$

This is the main model equation. The same master equation was derived in [8] in a different set-up for another biological application. This equation bears deep similarity to the Boltzmann equation of statistical physics.

**2.2. Symmetries of the model.** Integrating both sides of (2.5) over the variable  $\theta$  and using the normalization condition (2.1), we establish conservation of mass of filaments:

$$(2.6) \quad \int_{-\pi}^{\pi} f(\theta, t) d\theta = \text{const} = 1 \quad \text{for all } t \geq 0$$

(we normalize the total mass of filaments to be 1). The isotropic character of our model forces the following symmetry assumptions of the turning probability and frequency functions:

$$(2.7) \quad \eta(\theta) = \eta(-\theta), \quad w(\theta_1, \theta_2) = w(-\theta_1, -\theta_2).$$

The symmetry properties (2.7) have an important consequence. If  $f$  is a solution of (2.5), then  $g_{\pm}(\theta, t) := f(\Theta \pm \theta \text{ mod } 2\pi, t)$ , where  $\Theta$  is the direction of some arbitrary axis, are also solutions of (2.5) because

$$\begin{aligned} & \frac{\partial g_{\pm}}{\partial t}(\theta, t) \\ &= -f(\Theta \pm \theta, t) \int_{-\pi}^{\pi} \eta(\Theta \pm \theta - \theta_i) f(\theta_i, t) d\theta_i \\ & \quad + \int_{-\pi}^{\pi} \int_{-\pi}^{\pi} w(\theta_o - \Theta \mp \theta, \theta_o - \theta_i) \eta(\theta_o - \theta_i) f(\theta_o, t) f(\theta_i, t) d\theta_i d\theta_o \\ &= -g_{\pm}(\theta, t) \int_{-\pi}^{\pi} \eta(\theta - \theta_i) g_{\pm}(\theta_i, t) d\theta_i \\ & \quad + \int_{-\pi}^{\pi} \int_{-\pi}^{\pi} w(\theta_o - \theta, \theta_o - \theta_i) \eta(\theta_o - \theta_i) g_{\pm}(\theta_o, t) g_{\pm}(\theta_i, t) d\theta_i d\theta_o. \end{aligned}$$

Thus, the differential-integral equation is invariant under rotations and inversions. This yields also that reflectional symmetries of initial distributions are conserved in time.

**2.3. Examples of turning rates and interaction frequencies.** In the following we will give some examples of frequency functions and turning probabilities. Generally,  $g_\sigma$  with deviation  $\sigma > 0$  will denote either the periodic Gaussian or the normalized step function:

$$(2.8a) \quad g_\sigma(\theta) = \frac{1}{\sqrt{2\pi}\sigma} \sum_{z \in \mathbb{Z}} \exp\left(-\frac{1}{2} \left(\frac{\theta + 2\pi z}{\sigma}\right)^2\right), \quad \theta \in (-\pi, +\pi),$$

or

$$(2.8b) \quad g_\sigma(\theta) = \begin{cases} \frac{1}{2\sigma}, & |\theta| < \sigma (\leq \pi), \\ 0, & \sigma \leq |\theta| \leq \pi. \end{cases}$$

The analysis of the following sections shows that only a small number of features of  $g_\sigma$  are essential for the general qualitative behavior of the model. One of these features is, e.g., the fact that the Fourier transform of  $g_\sigma$  converges to 1 for small deviation.

We choose the turning probability function in the form

$$(2.9) \quad w(\theta_o - \theta_n, \theta_o - \theta_i) := g_\sigma((\theta_o - \theta_n) - v(\theta_o - \theta_i)).$$

With highest probability a filament turns from angle  $\theta_o$  to angle

$$(2.10) \quad \theta_n = \theta_o - v(\theta_o - \theta_i)$$

as a result of an interaction with a fiber at angle  $\theta_i$ ; see Figure 1. So  $v(\theta)$  is the average angle of turning as a function of the interaction angle  $\theta$ . We call  $v$  the *turning function*. To satisfy the symmetry assumptions (2.7), the turning function must be odd; i.e.,  $v(\theta) = -v(-\theta)$ . The parameter  $\sigma > 0$  is the deviation of the turning angle; we call this parameter the *uncertainty of turning*. The greater  $\sigma$ , the less exact alignment takes place (for example, when the rod domains of actin-binding proteins are long and flexible). When  $\sigma \ll 1$ , alignment is almost exact; the turning angle is determined by the interaction (e.g., when the rod domains of actin-binding proteins are short).

We introduce a few qualitatively different turning functions. In all examples the parameter  $\kappa$ ,  $0 \leq \kappa \leq 1$ , is a measure for the magnitude of the turning angle. We call  $\kappa$  the *attractivity coefficient*.

1. a.  $v(\theta) = \kappa \sin(\theta)$ : attracting interaction. At all interaction angles the angle between two filaments decreases according to the law of the resultant force.

b.  $v(\theta) = \kappa\theta$ : attracting interaction. Here, the directions of two filaments converge proportional to the interaction angle. This turning function increases with the interaction angle, and it is discontinuous at the interaction angle  $\pi$ .

Both interactions 1a and 1b are asymptotically equivalent at small interaction angles. In general, a turning function  $v$  is called *attracting* if  $0 < v(\theta) < \theta$  for all  $0 < \theta < \pi$ ; i.e., two filaments turn toward each other. After interaction and turning, their mutual angle is smaller than before.

2.  $v(\theta) = \frac{\kappa}{2} \sin(2\theta)$ : mixed attracting/repulsing interaction. Filaments converge at acute interaction angles and diverge at obtuse angles (i.e., convergence to rear end of interaction partner).

3.  $v(\theta) = -\frac{\kappa}{2} \sin(2\theta)$ : mixed attracting/repulsing interaction. Filaments diverge at acute interaction angles and converge at obtuse angles.

If  $\kappa = 0$ , there is no biased turning. If  $\kappa \simeq 0$ , we have the “weak” limit; at each interaction mutual angles converge (or diverge) just a little bit.

To model parallel and orthogonal binding configurations, we will use three different frequency functions. The parameter  $\rho > 0$  is a measure for the *effective range* at which filaments interact with each other. Note that  $g_\rho$  is the second Gaussian or step function in the equation but that  $\sigma$  and  $\rho$  have quite different meanings in the model.

1.  $\eta(\theta) = \frac{1}{2\pi}$ : the frequency of turning is angle independent;
2.  $\eta(\theta) = g_\rho(\theta)$ : the frequency of turning is larger at small interaction angles and smaller at larger angles;
3.  $\eta(\theta) = \frac{1}{2}(g_\rho(\theta - \frac{\pi}{2}) + g_\rho(\theta + \frac{\pi}{2}))$ : the frequency of turning is greater at orthogonal angles and smaller for parallel and antiparallel fibers.

Altogether we have three parameters characterizing these models: the effective interaction range  $\rho$ , the uncertainty of turning  $\sigma$ , and the attractivity coefficient  $\kappa$ .

**3. Linear stability analysis.** It is easy to check that the homogeneous angular distribution (no angular order)  $f(\theta) = \text{const} = \frac{1}{2\pi}$  is a stationary solution of the model equation (2.5). Here we analyze the linear stability of this steady state under small perturbations. We represent the angular distribution in the form

$$f = \frac{1}{2\pi} + \tilde{f}, \quad \int_{-\pi}^{\pi} \tilde{f}(\theta) d\theta = 0, \quad |\tilde{f}| \ll 1.$$

(Because of mass conservation (2.6) in our model, the homogeneous distribution is neutrally stable under constant perturbations.) Plugging this expression into (2.5) and keeping only linear terms, we obtain the linearized equation

$$(3.1) \quad \frac{\partial \tilde{f}}{\partial t} = -\tilde{f} - \eta * \tilde{f} + I * \tilde{f},$$

where the symbol  $*$  denotes the convolution of two functions:

$$(\eta * \tilde{f})(\theta) = \int_{-\pi}^{\pi} \eta(\theta - \psi) \tilde{f}(\psi) d\psi$$

and

$$I(\theta) := \int_{-\pi}^{\pi} \eta(\psi) (w(\theta, \psi) + w(\theta + \psi, \psi)) d\psi.$$

The rotational invariance of the model (see section 2.3) is reflected in the fact that all operators in (3.1) are convolutions. This, in turn, implies that  $\{\exp(il\theta)\}$ ,  $l \in \mathbb{Z}$ , is a complete orthogonal system of eigenfunctions for the right-hand side of (3.1). Therefore, Fourier transformation yields the following linear system of equations for the time dependent amplitudes  $\hat{f}_l$  of the perturbation modes  $\exp(il\theta)$ :

$$(3.2) \quad \frac{d\hat{f}_l}{dt} = (-1 - \hat{\eta}_l + \hat{I}_l) \hat{f}_l =: c_l \hat{f}_l, \quad l \in \mathbb{Z},$$

where the linear growth rates of the perturbation modes,  $c_l$ , involve the  $l$ th Fourier coefficients,  $\hat{\eta}_l$ ,  $\hat{I}_l$ , of the functions  $\eta(\theta)$ ,  $I(\theta)$ , respectively. (Here we define  $\hat{f}_l := \int_{-\pi}^{\pi} f(\theta) e^{-il\theta} d\theta$  and  $\hat{\eta}_l$ ,  $\hat{I}_l$  analogously.)

Because of the symmetry properties (2.7), the coefficients  $c_l$  are real, and  $c_l = c_{-l}$  for all  $l$ . The homogeneous solution is stable if for all wavenumbers  $l \geq 1$ , the eigenvalue  $c_l$  is negative, and it is unstable if there exists at least one  $l \geq 1$  such that  $c_l$  is positive. At most, finitely many eigenvalues can be positive because  $\hat{\eta}_l, \hat{I}_l \rightarrow 0$  for  $|l| \rightarrow \infty$ .

Let us first consider the case of purely random turning; i.e.,  $w = \text{const}$ . Then  $\hat{I}_l = 0, l \neq 0$ . Because of the positivity and normalization of the function  $\eta$ , we have the inequality  $|\hat{\eta}_l| < 1, l \neq 0$ . Then  $c_l = -1 - \hat{\eta}_l < 0$ , and the homogeneous distribution is stable. Thus, angle-independent interaction does not lead to order even if the frequency of interactions depends on mutual angles. This conclusion does not contradict some known facts, such as, for example, bacteria’s ability to move unidirectionally by changing the frequency of reorientation depending on their spatial position. In that case, the spatial inhomogeneity leads to the directionality of motion. In our case, we consider the isotropic dynamics in the angular space. Though at some angles filaments interact more frequently than at others, this alone does not lead to alignment, because the average reorientation angle of the pair of interacting filaments is arbitrary. Because of this rotational invariance there is no angular bias on the average. If some biochemical bias in the cytoplasm is introduced, and the rotational invariance is broken, then the angular dependence of the turning frequency alone could cause alignment.

Further, we consider the case of angle-biased turning  $w \neq \text{const}$  and angle-independent frequency of interaction  $\eta = \text{const} = \frac{1}{2\pi}$ . The criterion for instability then has the form

$$(3.3) \quad c_l = -1 + \frac{1}{2\pi}(\hat{w}_{l,0} + \hat{w}_{l,-l}) > 0 \quad \text{for some } l > 0,$$

where  $\hat{w}_{k,l} = \int_{-\pi}^{\pi} \int_{-\pi}^{\pi} e^{-ik\psi_1} e^{-il\psi_2} w(\psi_1, \psi_2) d(\psi_1, \psi_2)$ . The coefficients  $\hat{w}_{l,0}, \hat{w}_{l,-l}$  can be explicitly calculated for turning probability function (2.9):

$$(3.4) \quad \begin{aligned} 1 + c_l &= \frac{1}{2\pi} \int_{-\pi}^{\pi} \int_{-\pi}^{\pi} g_{\sigma}(\psi_1 - v(\psi_2)) (1 + e^{-i(-l)\psi_2}) e^{-il\psi_1} d\psi_1 d\psi_2 \\ &= \frac{1}{2\pi} \hat{g}_{\sigma l} \int_{-\pi}^{\pi} (\cos(lv(\psi)) + \cos(l(\psi - v(\psi)))) d\psi. \end{aligned}$$

Here

$$(3.5a) \quad \hat{g}_{\sigma l} = \frac{\sin(l\sigma)}{l\sigma} \quad \text{for the step function}$$

and

$$(3.5b) \quad \hat{g}_{\sigma l} = e^{-\frac{1}{2}(2\pi\sigma l)^2} \quad \text{for the periodic Gaussian.}$$

An analysis of expressions (3.4)–(3.5) leads us to the following conclusions:

1. The uncertainty of turning  $\sigma$  has to be small enough in order for an instability to occur. This means that turnings must be precise enough; otherwise, any ordering would be smeared out by stochastics.

2. If  $v$  is identically zero (i.e., no turning, e.g., attractivity coefficient  $\kappa = 0$ ), then the homogeneous solution is always stable.

3. In the case of attracting turning function, the first mode becomes unstable for small enough uncertainty of turning. Because  $\hat{g}_{\sigma l}$  converges to 1 for small  $\sigma$ , we

have to show that  $\int_{-\pi}^{\pi} (\cos v(\psi) + \cos(\psi - v(\psi))) d\psi > 2\pi$ . For attracting turning function  $v$ , we have

$$\begin{aligned} \int_{-\pi}^{\pi} (\cos v(\psi) + \cos(\psi - v(\psi))) d\psi &= 2 \int_{-\pi}^{\pi} \cos\left(\frac{1}{2}\psi\right) \cos\left(v(\psi) - \frac{1}{2}\psi\right) d\psi \\ &> 2 \int_{-\pi}^{\pi} \cos^2\left(\frac{1}{2}\psi\right) d\psi = 2\pi. \end{aligned}$$

However, even for attracting turning functions, the first mode needs not be the largest mode. In Appendix A we construct a turning function for which higher mode numbers can be larger than the first mode.

Figures 2a,b show the graphs of  $\kappa \mapsto \bar{\sigma}_l(\kappa)$  with  $c_l(\kappa, \bar{\sigma}_l(\kappa)) = 0$  for the first few  $l$  when  $v$  is the linear attracting turning function (Figure 2a) and a mixed attracting/repulsing turning function (Figure 2b), respectively, and  $\kappa$  is the attractivity coefficient. Below the curves the eigenvalue  $c_l = c_l(\kappa, \sigma)$  is positive; i.e., for these parameter values  $(\kappa, \sigma)$  the corresponding wavenumbers  $l$  are unstable.

For the linear turning function, Figure 2a, eigenvalues to even wavenumbers are negative for all  $\kappa$  and  $\sigma$ , hence the constant solution is stable with respect to perturbations of even mode numbers. Moreover, the (positive) linear growth rate of the first mode is the largest at all values of the parameters. Thus, one predicts that purely attracting interaction leads to alignment in a single direction. The function  $\bar{\sigma}_1(\kappa)$  has a maximum at  $\kappa = \frac{1}{2}$ , so alignment is the most effective when the average angle of turning is equal to half the initial mutual angle (effectively, the orientations of two filaments merge after turning). The plot's symmetry results from the fact that the behavior of the model with linear turning function is unchanged if  $\kappa$  is replaced with  $1 - \kappa$ .

Figure 2b shows that for the mixed attracting/repulsing turning function,  $v(\theta) = \frac{\kappa}{2} \sin(2\theta)$ , the second mode is the only one which becomes unstable for small uncertainty of turning. Therefore, one expects the formation of bundles with filaments in opposing orientations (i.e., two maxima of the distribution function at distance  $\pi$ ). The same figure (multiplied by 2 and with  $l = 1$  instead of 2) holds for the attracting turning function  $v(\theta) = \kappa \sin \theta$ . Interestingly, there is no degeneracy at  $\kappa = \sigma = 0$ , in contrast to the linear turning function for which infinitely many (odd) modes become unstable near the origin.

#### 4. Peak-like angular distribution in the case of attracting interaction.

**4.1. Stability of a single peak in the case of exact alignment.** The linear stability analysis of the preceding section has shown that for small uncertainty of turning,  $\sigma$ , the constant solution is unstable. Numerical calculations (see also section 5) show that as  $\sigma$  decreases, peaks become narrower. This leads to the plausible assumption that in the limiting case of  $\sigma \rightarrow 0$ , and with attracting interaction mechanisms, the resulting angular pattern would be that of complete alignment. Indeed, in this section we will demonstrate that in the case of purely attracting interaction, of angle-independent frequency of interaction (i.e.,  $\eta = \text{const}$ ), and of exact alignment (i.e.,  $\sigma = 0$ ), a single  $\delta$ -peak is a stable solution.

First, let us note that the functions  $g_\sigma$  (for both Gaussian and step function cases) converge to the delta distribution as  $\sigma \rightarrow 0$ ,  $g_\sigma \rightarrow \delta$ . We transform the integral on

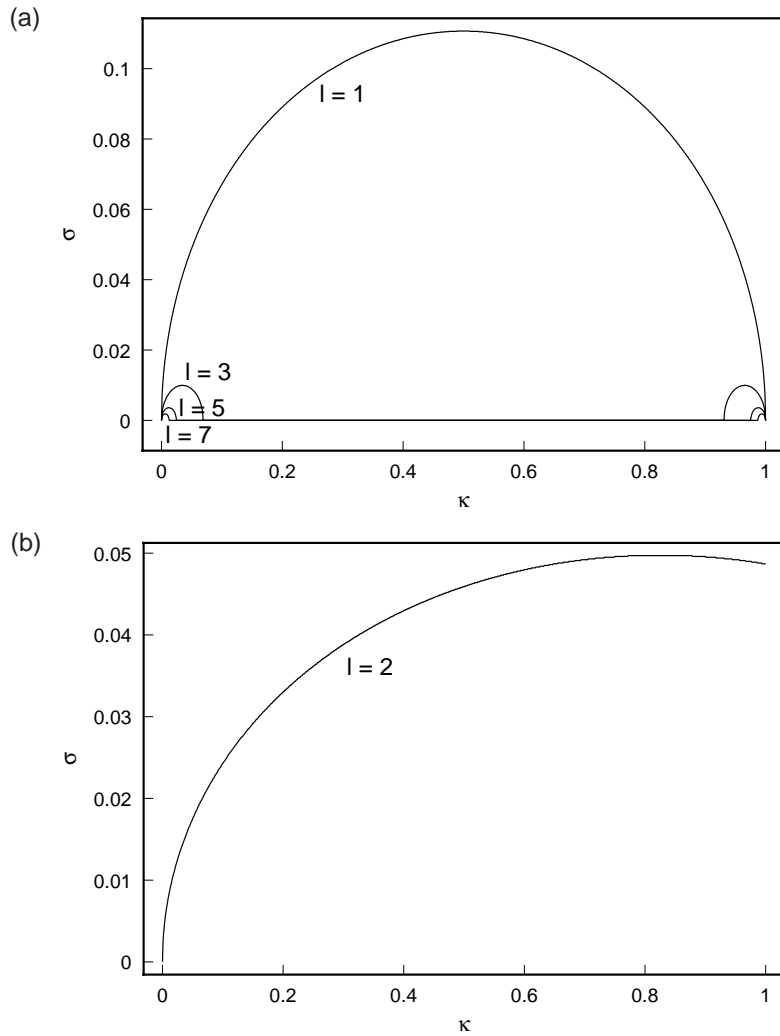


FIG. 2. For parameter values above the curves the rates  $c_l$  are negative (meaning that the constant solution is stable under perturbations of that wavenumber). For parameter values below the curves the rates  $c_l$  are positive (the homogeneous distribution is unstable under perturbations of the form described by that mode.) (2a) The level curves  $c_l(\sigma, \kappa) = 0$  ( $l = 1, 3, 5, 7$ ) for the case of unidirectional bundling ( $v(\psi) = \kappa\psi$ ;  $g_\sigma$  is the periodic Gaussian). All even modes are stable in this case. (2b) The level curve  $c_2(\sigma, \kappa) = 0$  for the case of mixed attracting/repulsing turning function ( $v(\psi) = \frac{\kappa}{2} \sin(2\psi)$ ;  $g_\sigma$  is the periodic Gaussian). All other modes are stable.

the right-hand side of (2.5) and let  $\sigma \rightarrow 0$ :

$$\begin{aligned}
 & \int_{-\pi}^{\pi} \int_{-\pi}^{\pi} g_\sigma(\theta_o - \theta - v(\theta_o - \theta_i)) f(\theta_o) f(\theta_i) d\theta_o d\theta_i \\
 &= \int_{-\pi}^{\pi} g_\sigma(\psi_1) \int_{-\pi}^{\pi} f(\theta - \psi_1 - v(\psi)) f(\theta - \psi_1 + \psi - v(\psi)) d\psi d\psi_1 \\
 &\xrightarrow{\sigma \rightarrow 0} \int_{-\pi}^{\pi} f(\theta - v(\psi)) f(\theta + (\psi - v(\psi))) d\psi =: A(f)(\theta).
 \end{aligned}$$

Hence, model equation (2.5) can be rewritten as

$$(4.1) \quad \frac{\partial f}{\partial t} = \frac{1}{2\pi} (-f + A(f)),$$

where  $f$  may be a distribution and the distribution  $A(f)$  acts on a test function  $\Phi \in C^\infty(R)$  as follows:

$$(4.2) \quad \langle A(f)(\theta), \Phi(\theta) \rangle := \langle f(\theta), \langle f(\psi), \Phi(\theta + v(\psi - \theta)) \rangle_\psi \rangle_\theta.$$

( $\langle f, \Phi \rangle$  denotes the action of a distribution on a test function.) After suitably rescaling time, (4.1) becomes

$$(4.3) \quad \frac{\partial f}{\partial t} = -f + A(f).$$

We want to show that a single delta peak,  $\delta(\theta - \bar{\theta})$ , is a stationary solution of (4.3). Because of the translational invariance of the problem, it suffices to show that  $\delta(\theta)$  is a stationary solution; i.e.,  $A(\delta) = \delta$ . This is easy to see because  $v(0) = 0$ , and therefore,

$$\begin{aligned} \langle A(\delta)(\theta), \Phi(\theta) \rangle &= \langle \delta(\theta), \langle \delta(\psi), \Phi(\theta + v(\psi - \theta)) \rangle \rangle \\ &= \langle \delta(\theta), \Phi(\theta + v(-\theta)) \rangle = \Phi(0) = \langle \delta(\theta), \Phi(\theta) \rangle. \end{aligned}$$

In order to investigate the stability of this single peak, we linearize the differential integral equation (4.3). We represent the perturbed peak-like solution in the form  $f = \delta + \tilde{f}$ , where  $\langle \tilde{f}, 1 \rangle = 0$ , and keep further only terms of linear order in  $\tilde{f}$ . The linearized equation has the form

$$(4.4) \quad \frac{\partial \tilde{f}}{\partial t} = -\tilde{f} + L_v(\tilde{f}) + L_{\text{id}-v}(\tilde{f}),$$

where the operator  $L_v$  acts as follows:

$$(4.5) \quad \langle L_v(f)(\theta), \Phi(\theta) \rangle = \langle f(\theta), \Phi(v(\theta)) \rangle,$$

and  $L_{\text{id}-v}$  is defined analogously.

The linear equation (4.4) with initial distribution  $\tilde{f}(\cdot, 0) = \tilde{f}_0$  can be solved explicitly. This is done in Appendix B, where we further show that

$$\tilde{f}(\cdot, t) \rightarrow -\langle \tilde{f}_0(\theta), \theta \rangle \delta' \quad \text{for } t \rightarrow \infty$$

if the turning function  $v$  is attracting; i.e.,  $0 < v(\theta) < \theta$  for  $0 < \theta < \pi$ .

We define  $\theta_\infty := \langle \tilde{f}_0(\theta), \theta \rangle = \langle f(\theta, 0), \theta \rangle$  for  $f(\cdot, 0) = \delta + \tilde{f}_0$ . Thus, the solution  $f(t) = \delta + \tilde{f}(t)$  of (4.3) converges in linear approximation to

$$(4.6) \quad f(t) \rightarrow \delta - \theta_\infty \delta' = \delta(\cdot - \theta_\infty) + O(\theta_\infty^2) \quad \text{for } t \rightarrow \infty.$$

This proves that after a small perturbation the  $\delta$ -peak does not change its shape but moves to the new angle  $\theta_\infty$  (which is close to the 0-angle because of the smallness of the perturbation). If the perturbation  $\tilde{f}_0$  is even, then  $\theta_\infty = \langle \tilde{f}_0(\theta), \theta \rangle = 0$ , and the peak remains unmoved.

**4.2. The shape of the peak.** We expect that in the case of almost exact alignment  $0 < \sigma \ll 1$  the angular distribution has the form of a narrow peak. In order to find the shape of this peak, we solve approximately (with an error of the order  $\exp(-1/\sigma)$ ) the stationary integral equation:

$$(4.7) \quad -f(\theta) + \int_{-\pi}^{\pi} \int_{-\pi}^{\pi} g_{\sigma}(\theta_o - \theta - v(\theta_o - \theta_i)) f(\theta) f(\theta_o) d\theta_i d\theta_o = 0.$$

Introducing the new variable  $x = \frac{\theta}{\sigma}$ , we rescale the angular distribution. Letting the rescaled limits of integration be equal to  $\pm\infty$  (which at small  $\sigma$  gives only exponentially small error), we obtain the approximate integral equation:

$$(4.8) \quad \tilde{f}(x) = \int_{-\infty}^{\infty} \int_{-\infty}^{\infty} G_1(x_o - x - v(x_o - x_i)) \tilde{f}(x_i) \tilde{f}(x_o) dx_i dx_o.$$

It is easy to check that this equation has a solution of the following form provided  $v(\theta) = \kappa\theta$ :

$$(4.9) \quad \tilde{f}(x) = G_{\epsilon}(x), \quad \epsilon = \frac{1}{\sqrt{2\kappa(1-\kappa)}},$$

where  $G_{\epsilon}$  is the Gaussian on  $\mathbb{R}$  with deviation  $\epsilon$ . Hence, at small uncertainty of turning,  $\sigma$ , the approximate stationary angular distribution has the Gaussian shape

$$(4.10) \quad f(\theta) = A \exp\left(-\frac{\kappa(1-\kappa)\theta^2}{\sigma^2}\right), \quad A = \frac{\sqrt{\kappa(1-\kappa)}}{\sqrt{\pi}\sigma},$$

and the approximation error is exponentially small. The peak is narrow: the width of the distribution is equal to  $\frac{\sigma}{\sqrt{2\kappa(1-\kappa)}}$  (remember that  $\kappa$  is fixed and  $\sigma \rightarrow 0$ ). We conjecture that for small  $\sigma$  this peak-like distribution is stable.

Let us consider in more detail the case of small attractivity coefficient  $\kappa \rightarrow 0$  and almost exact alignment  $\sigma \rightarrow 0$ . In this case the approximation used in this section is valid if  $\sigma$  is small compared to  $\kappa$  in the following sense. Let, e.g.,

$$\sigma = \sigma(\kappa) = \kappa^{\gamma}.$$

Then the above analysis can be done analogously with rescaling  $x = \theta/\kappa^{\gamma}$ , and the solution (4.10) again has Gaussian form with deviation

$$(4.11) \quad \frac{\kappa^{(\gamma-\frac{1}{2})}}{\sqrt{2(1-\kappa)}};$$

i.e., the width of the peak of the distribution is of order  $\kappa^{(\gamma-\frac{1}{2})}$ . The approximations of this subsection are valid only if this width is small compared to  $\pi$  or if  $\gamma > \frac{1}{2}$ . Independently of the linear stability analysis, this confirms the conclusion that as the attractivity coefficient becomes smaller, making alignment less prominent, the turning has to become more exact in order for the angular pattern to exist. It is interesting that the scaling law (4.11) relates to the corresponding result of the linear stability analysis: if at small  $\sigma$  and  $\kappa$  the inequality  $\sigma > a\kappa^{\frac{1}{2}}$  holds (where  $a$  is some constant of order 1), then the homogeneous distribution is stable and no pattern evolves. If, on the other hand, the inverse inequality holds, the stability of the constant solution is broken.

**5. Results of numerical simulations.** In this section we present numerical results in order to complement the analytical ones. The discrete model which we used for computer simulations is introduced in [8], so we do not repeat the derivation here. The following system of ordinary differential equations was suggested as an approximation to the integrodifferential equation (2.4):

$$(5.1) \quad \frac{\partial y_i}{\partial t}(t) = -y_i \sum_{j=0}^{n-1} \sum_{k=0}^{n-1} w_{k,i-j} \eta_{i-j} y_j + \sum_{j=0}^{n-1} \sum_{k=0}^{n-1} w_{j-i,j-k} \eta_{j-k} y_j y_k$$

for  $i = 0, \dots, n - 1$ , where  $y_i = f(2\pi i/n)$ . The vector  $(\eta_i)_{i=0, \dots, n-1}$  and the matrix  $(w_{i,j})_{i,j=0, \dots, n-1}$  are discretized versions of the functions  $\eta$  and  $w$ ; e.g.,  $w_{ij} = w(2\pi i/n, 2\pi j/n)$ . The periodicity of the functions is reflected by the conditions  $\eta_i = \eta_{i+n}$  and  $w_{i+n,j} = w_{i,j} = w_{i,j+n}$ . We solve the ordinary differential equations with an Euler scheme starting with a randomly chosen periodic continuous distribution.

For all our simulations we took  $w(\theta_1, \theta_2) = g_\sigma(\theta_1 - v(\theta_2))$  as in section 2.3. In all cases considered, we observed several common features:

1. A fast symmetrization of the initial distributions was achieved during the first few time steps. This means that at least a reflection symmetry evolved (on  $S^1$ ) with reflection points at a distance of  $\pi$ .
2. For large uncertainty of turning  $\sigma$ , solutions converged to the homogeneous distribution (see [6] for an analytical proof of this fact). Near the bifurcation point the solutions converged to stationary distributions which have several mild humps. The number of humps depends on the spectral properties of the turning frequency  $\eta$  and the turning function  $v$ .
3. The smaller the uncertainty of turning  $\sigma$  was, i.e., the more exact the alignment of two filaments was, the narrower and the higher the peak(s) were in the evolving angular distribution.

In the first group of simulations we took angle-independent frequency of turning  $\eta = 1/2\pi$ .

In the case of attracting turning functions,  $v(\theta) = \kappa \sin(\theta)$  and  $v(\theta) = \kappa\theta$ , and with  $\sigma$  small enough, the evolving stationary distributions had a single maximum (Figure 3) (except when the initial distribution had too much symmetry; see section 2.2) even if several eigenvalues besides the first were positive.

The shape of this distribution was independent of the initial conditions, with the position of the maximum depending on the initial distribution in an unknown way. Usually the maximum evolved near the biggest hump of the initial distribution: a concentration of filaments around some direction behaves like an attractor.

In the case of the mixed attracting and repulsing interaction, characterized by the continuous turning function  $v(\theta) = \frac{\kappa}{2} \sin(2\psi)$  (angular convergence at acute angles and divergence at obtuse angles) and with  $\sigma$  (dependent on  $\kappa$ ) small enough, the solutions converged to a double humped stationary distribution (Figure 4).

For large time the two peaks in the angular distribution had about equal heights. The angle between the two peaks was close to  $\pi$ . The simulations revealed nontrivial transitional dynamics of the angular distribution. Already within the first few time steps, two humps of unequal height evolved. From then on the shape of the solution did not change significantly. Nevertheless, the two humps grew in height at about the same rate until the development seemed to slow down at times of order 100 (in time units). Thereafter, the bigger hump shrank and the smaller one grew very slowly until the two maxima became almost equal at times of order 1000. The bigger the

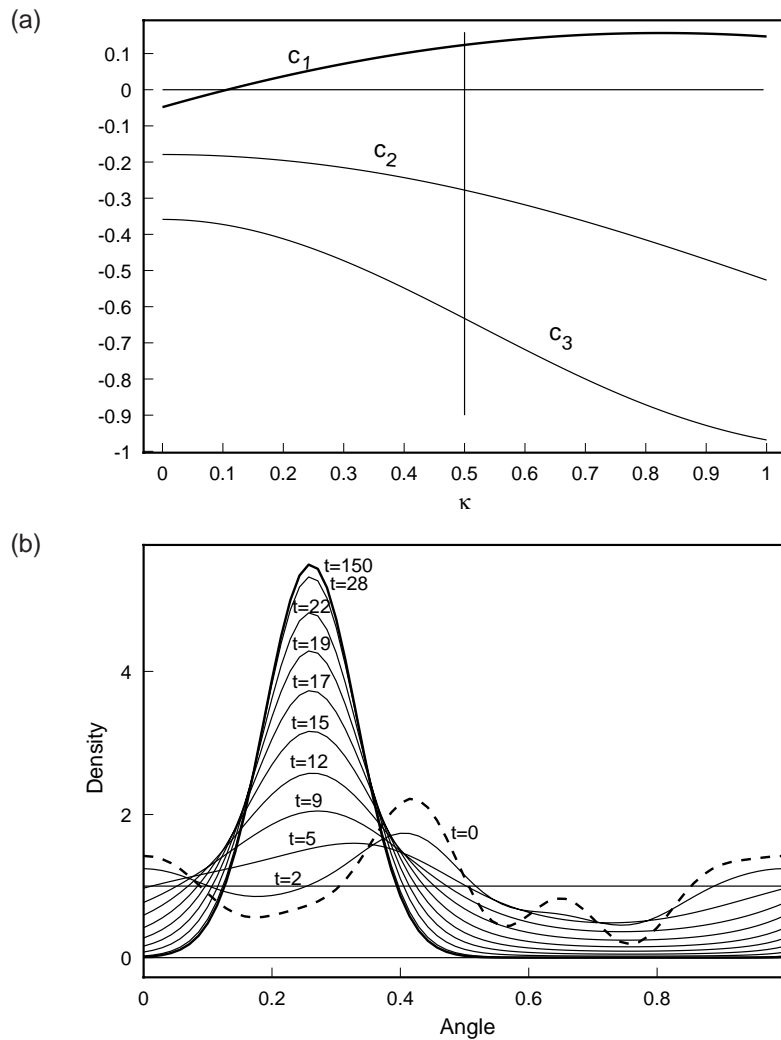


FIG. 3. Total alignment in one direction in the case of an attracting turning function. The first three eigenvalues are plotted in Figure 3a as functions of the attractivity coefficient  $\kappa$ . The first unstable mode is the first one. The numerical solution of model equation (5.1) is shown in Figure 3b. For the simulation we used a second-order Euler scheme with variable time steps on 70 grid points. The initial density (thick dashed line) was generated randomly with total mass equal to 1. The parameter functions and values are  $\eta = 1$ ,  $v(\psi) = \frac{\kappa}{2\pi} \sin(2\pi\psi)$ ,  $\kappa = 0.5$ , and  $\sigma = 0.05$ . Then  $c_1 = 0.12$ . Note that we scaled the length of  $S^1$  to 1.

parameter  $\sigma$  was chosen, the faster the two humps reached equal height (there was more exchange between the two angular aggregation centers).

Next, we undertook a group of simulations with angle dependent frequency of turning. The frequency of interaction function was taken to be the periodic Gaussian  $\eta = g_\rho$  (fibers interact frequently at small angles), and we have chosen the discontinuous turning function  $v(\theta) = \kappa\theta$  describing attracting interaction. The eigenvalues  $c_l$  of (12) were calculated numerically. One of the conclusions was that for instability to

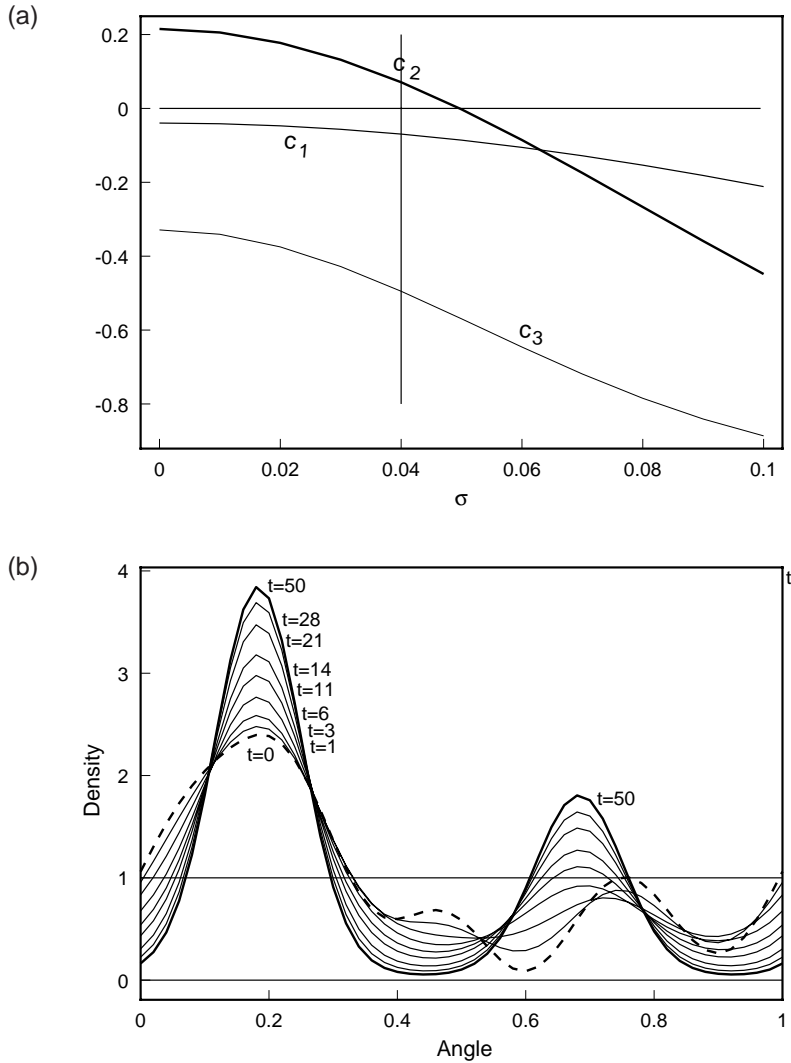
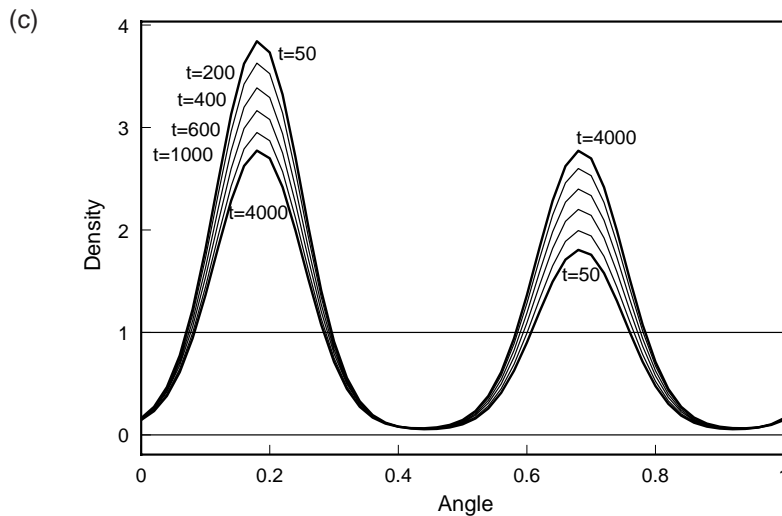


FIG. 4. Pattern of alignment in two directions in the case of mixed attracting/repulsing actin-actin interaction. Two filaments converge in the angular space if their interaction angle is in the range  $(-\frac{\pi}{2}, \frac{\pi}{2})$  ( $(-\frac{1}{4}, \frac{1}{4})$  at the figure) and diverge if the interaction angle is obtuse. In Figure 4a the first three eigenvalues are plotted as functions of the uncertainty of turning,  $\sigma$ . Only the second mode is unstable. The parameter functions and values are:  $\eta = 1$ ,  $(v(\psi) = \frac{\kappa}{4\pi} \sin(4\pi\psi))$ , ( $\kappa = 0.8$ , and  $\sigma = 0.04$ ). Note that we scaled the length of  $S^1$  to 1. Then  $c_1 = -0.069$  and  $c_2 = 0.071$ . (4b) For the simulation we used a second-order Euler scheme with variable time steps on 50 grid points. The randomly chosen initial density (thick dashed line) with mass 1 is shown and the solution at several times up to time 50 (at which time the solution is shown with the thick line in (4b) and (4c)). At that time the left peak reaches its maximum. (4c) The higher left peak starts to shrink while the smaller right peak continues to grow. The solution converges to a stationary distribution with two peaks of equal height at the mutual angle  $\pi$ .

FIG. 4. (*cont.*).

occur, the parameter  $\sigma$  must be smaller than  $\rho$ , otherwise the range of interaction  $\rho$  is smaller than the exactness of alignment  $\sigma$  and no pattern can exist. We observed that as both parameters  $\rho$  and  $\sigma$  were decreased, the first mode became unstable first. The new feature in comparison to the first case was that higher-mode eigenvalues could become larger than smaller-mode eigenvalues.

Figure 5 shows that even if the second-mode eigenvalue was bigger than the first one, eventually only a single peak survived though transiently two humps developed.

Indeed, early in the development two humps evolved, one of which usually grew faster than the other one. The two peaks were approximately at an angle  $\pi$  from each other, and they coexisted for some time then moved toward each other. At this same time the smaller peak began to flatten out, while the larger peak slowed down.

If the values of both parameters  $\rho$  and  $\sigma$  were very small (providing many unstable modes), then a large number of approximately equidistantly spaced humps evolved at the beginning of the simulations. The number of humps depended mainly on the parameter values and on the initial distribution. The characteristic relaxation times increased rapidly, and rarely (depending on initial conditions) convergence to the single peak could be observed.

Finally, we simulated orthogonal alignment choosing  $\eta(\theta) = \frac{1}{2}(g_\rho(\theta - \frac{\pi}{2}) + g_\rho(\theta + \frac{\pi}{2}))$  (the filaments interact with high probability if they are orthogonal to each other) and the continuous turning function  $v(\theta) = -\frac{\pi}{2} \sin(2\theta)$  (cells converge at obtuse angles and diverge at acute angles). The numerical simulations showed (in agreement with the calculations of the eigenvalues of the corresponding stability problem) that four equally spaced peaks' distribution evolved (Figure 6).

**6. Discussion.** The analysis of our model confirms that biologically feasible types of actin-actin interaction lead to the observed angular patterns. The main qualitative result of our work is that bifurcation from angular disorder to alignment occurs when the uncertainty of turning is smaller than some critical value. This critical uncertainty decreases to zero in cases of both no turning at all and exact exchange. Also, the model demonstrates how a single equation with quadratic nonlinearities and turning to “intermediate” angles can provide pattern formation. (The earlier model

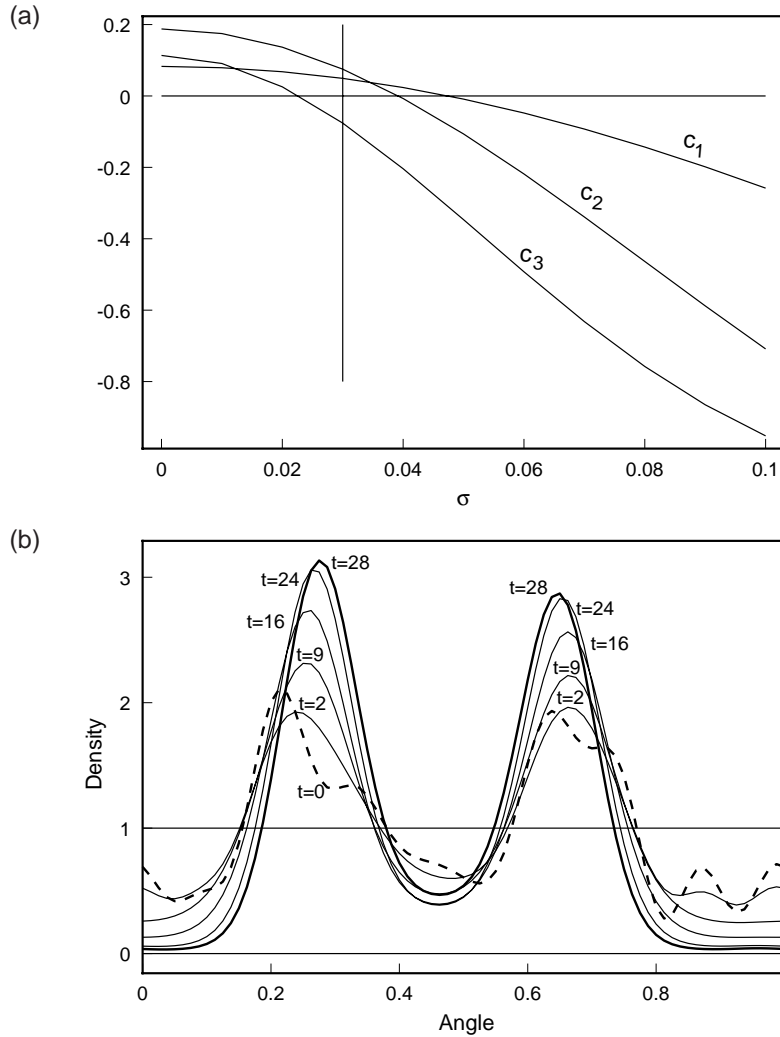
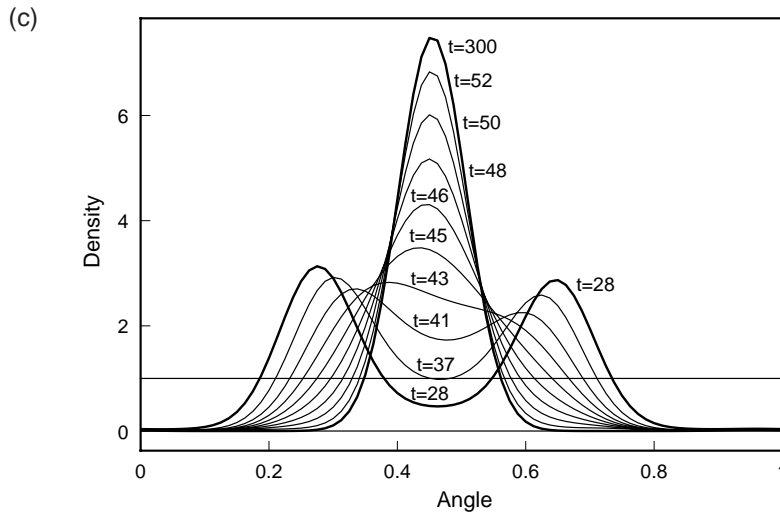


FIG. 5. Alignment to a single direction in the case of an attracting turning function through transitory states with two peaks in the angular distribution. Figure 5a shows the first three eigenvalues as functions of the uncertainty of turning  $\sigma$ . For small  $\sigma$  three eigenvalues are positive, and higher-mode eigenvalues may be larger than the first one. All other modes are stable. The parameter functions and values were  $\eta = g_p$ ,  $\rho = 0.1$ ,  $v(\psi) = \kappa\psi$ ,  $\kappa = 0.5$ , and  $\sigma = 0.03$ . Note that we scaled the length of  $S^1$  to 1. Then first and second modes are unstable:  $c_1 = 0.049$ ,  $c_2 = 0.075$ . Note that  $c_1 < c_2$ . (5b) For the simulation we used a second-order Euler scheme with variable time steps on 80 grid points. The initial density with mass 1 is shown with the thick dashed line. Initially two predominant directions of alignment evolve. At time 28 both peaks reach their maximal height (the solution at time 28 is shown with a thick line in (5b) and (5c)). (5c) Then the two peaks shrink while moving toward each other. They merge and a single peak develops. Note that the scaling on the density axis is different in Figures (5b) and (5c).

FIG. 5. (*cont.*).

of [2] gives nontrivial results only with two equations; see also [4].

The distinctive feature of our model is that the physical origin of disorder is the uncertainty in the angle of turning (caused by the flexibility of the actin-binding proteins) rather than angle-independent rotational diffusion. Of course, a too-low amount of actin-binding protein (i.e.,  $w \approx 1$ ), and, therefore no biased turning, also leads to disorder.

As long as only one mode is unstable near the constant solution, its number often predicts the number of directions of alignment or the number of maxima of the stationary solution which will evolve globally. We confirmed this prediction with the help of numerical simulations. In fact, a detailed bifurcation analysis [6] shows that near the first bifurcation, the stationary solution is of the form  $\frac{1}{2\pi} + \frac{c_1 c_2}{A} \cos(2\pi\theta)$ , where  $c_1 > 0$  is the eigenvalue of the bifurcating first mode,  $c_2 < 0$  is the eigenvalue of the second mode, and  $A$  is a constant. Linear stability analysis and numerical simulations also agree in the cases of bipolar and orthogonal alignment.

Numerical calculations have shown that the mode which becomes unstable first, in general, dominates the angular distribution on long time scales even if other modes are also unstable. We proved the stability of peak-like distributions in the case of exact alignment, attracting turning mechanism and constant frequency function,  $\eta$ . We conjecture that (with these assumptions) this peak is the *only* nontrivial *stable* stationary solution and that this holds true also if the frequency function is non-constant and nonzero everywhere. The second conjecture is that the stability and uniqueness of the peak-like stationary solution also holds for  $0 < \sigma \ll 1$ .

The smaller the turnings are, the more modes are unstable, which makes it hard to interpret the results of the linear stability analysis. Numerical simulations demonstrate that in this situation several “aggregation” centers in the angular distribution develop in the beginning. Later, the neighboring centers can merge. Merging consists of two processes: drifting of the centers toward each other, and the changing of the heights of the corresponding peaks. The time scales of convergence to the stable angular distribution may be very large. To treat this problem mathematically one has to perform a multiscale perturbation analysis. At biologically realistic times, the sta-

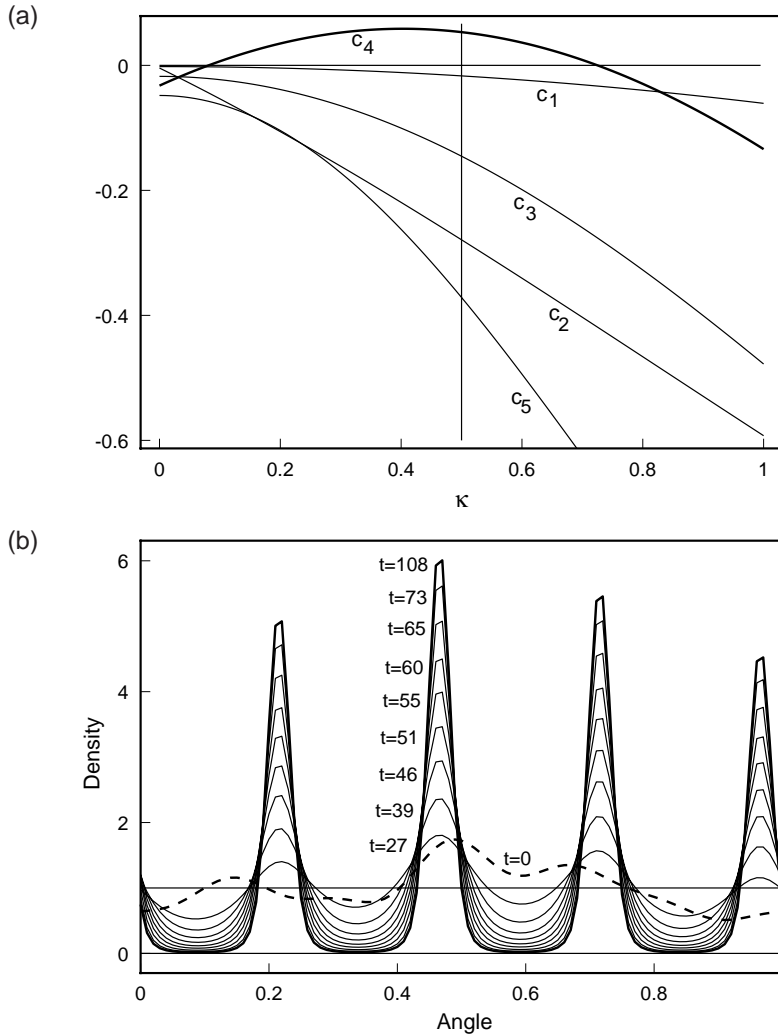
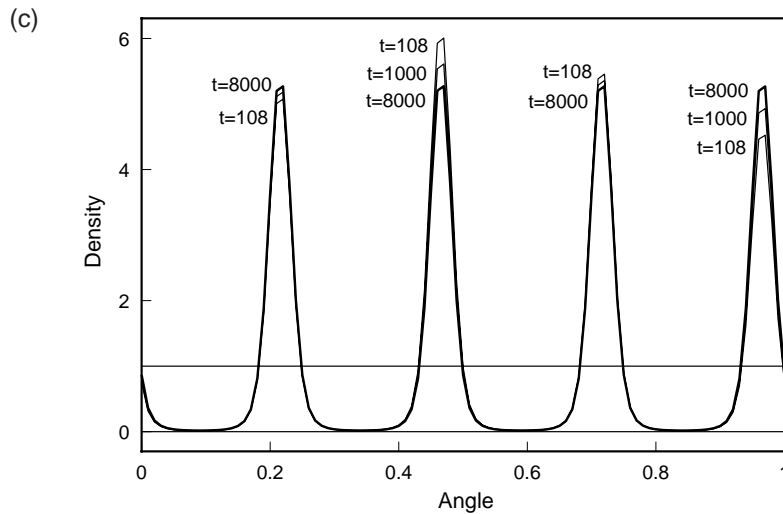


FIG. 6. Formation of four directions of alignment in the case of attraction toward an orthogonal configuration (specific mixed attracting/repulsing actin-actin interaction). Two filaments converge in the angular space if their interaction angle is obtuse and diverge if this angle is acute. In Figure 6a eigenvalues for the first five modes are plotted as functions of the attractivity coefficient  $\kappa$ . All modes except the fourth mode are stable. The parameter functions and values are ( $g_\rho$  is the periodic Gaussian)  $\eta(\psi) = \frac{1}{2}(g_\rho(2\pi(\psi - \frac{1}{2})) + g_\rho(2\pi(\psi + \frac{1}{2})))$ ,  $\rho = 0.1$ ,  $v(\psi) = -\frac{\kappa}{4\pi} \sin(4\pi\psi)$ ,  $\kappa = 0.5$ , and  $\sigma = 0.01$ . Then  $c_4 = 0.05$ . We used a second-order Euler scheme with variable time steps on 100 grid points. Note that we scaled the length of  $S^1$  to 1. (6b) The randomly chosen initial density (thick dashed line) with mass 1 is shown as well as the solution at several times up to time 108. At that time the second peak reaches its maximum. (6c) The second and third peak shrink while the first and fourth peak continue to grow. The solution converges very slowly to a stationary distribution with four peaks of equal height at mutual angles  $\frac{\pi}{2}$ . At times near 6000 all peaks have about equal mass.

FIG. 6. (*cont.*).

ble angular distribution does not have time to evolve. Thus, for a long time, various quasi-stationary patterns may be observed.

The nature of the transitions between different types of angular order as a result of a change in the type of interaction (e.g., when the concentrations of different actin-binding proteins suddenly change) is especially interesting when the underlying symmetry changes. The characteristic time of transition to the new pattern depends on the symmetries of the initial and final interactions (and on which of the symmetries is the higher one). In fact numerical simulations (which we do not present here in detail) show that the transition from four to two peaks goes through a transitory homogeneous distribution and is faster than the inverse transition when two new peaks appear.

**Appendix A.** The following example is due to M. Stoll [19]. Define

$$v(\theta) = \begin{cases} \frac{1}{2}\theta & \text{for } |\theta| < \Theta, \\ 0 & \text{for } \Theta \leq |\theta| < \pi. \end{cases}$$

Figure 7 shows the graphs of  $\Theta \mapsto \bar{\sigma}_l(\Theta)$ , where  $c_l(\Theta, \bar{\sigma}_l(\Theta)) = 0$  for  $l = 1, 2, 3$ , and  $\Theta \mapsto \bar{\sigma}_{kl}(\Theta)$ , where  $c_k(\Theta, \bar{\sigma}_{kl}(\Theta)) = c_l(\Theta, \bar{\sigma}_{kl}(\Theta))$  for  $(k, l) = (1, 2), (1, 3)$ . Straightforward calculations lead to explicit formulas for  $c_l(\Theta, \sigma)$ ,  $\bar{\sigma}_l(\Theta)$ , and  $\bar{\sigma}_{kl}(\Theta)$ .

Filaments interact at all angles (because  $\eta = \text{const}$ ) but they do not turn at interaction angles larger than  $\Theta$ . In actual fact the interaction radius is restricted. Small interaction radius favors the (at least initial) formation of several aggregation centers. This explains the large higher modes.

Note that this turning function is not attracting, according to the definition. However, a suitable and sufficiently small (continuous) perturbation of  $v$  leads to an attracting turning function, while the qualitative features of Figure 7 are preserved.

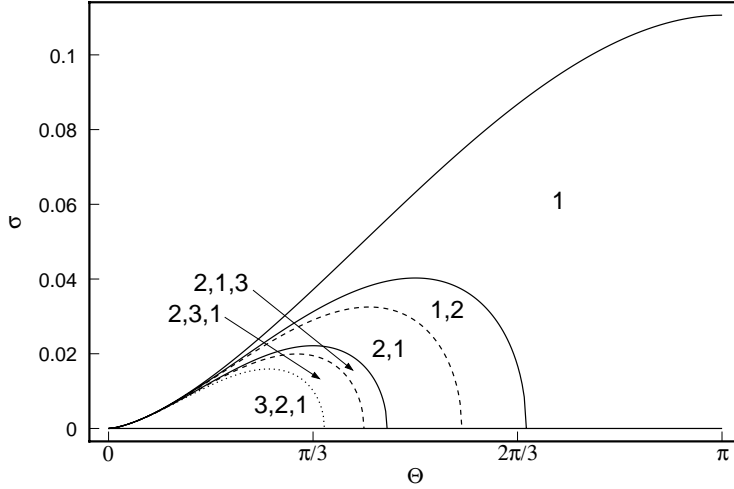


FIG. 7. The curves  $\bar{\sigma}_l$  for  $l = 1, 2, 3$  (solid lines) and  $\bar{\sigma}_{kl}$  for  $(k, l) = (1, 2), (1, 3)$  (dashed lines) and  $(k, l) = (2, 3)$  (dotted line). The turning function is defined in Appendix A, and  $g_\sigma$  is the periodic Gaussian. The numbers denote which mode number is unstable, the numbers' order shows the relative size of the eigenvalues (e.g., 2, 1, 3 means that  $c_2 > c_1 > c_3 > 0$ ).

**Appendix B.** The explicit solution of (4.4) for an initial distribution  $\tilde{f}_0$  can be found in the following way:

$$\begin{aligned} \tilde{f}(\cdot, t) &= e^{t(-\text{id} + L_v + L_{\text{id}-v})}(\tilde{f}_0) \\ &= e^{-t} e^{t(L_v + L_{\text{id}-v})}(\tilde{f}_0) = e^{-t} \sum_{k=0}^{\infty} \frac{t^k}{k!} (L_v + L_{\text{id}-v})^k(\tilde{f}_0), \end{aligned}$$

where the second equality holds because  $\text{id}$  and  $L_v + L_{\text{id}-v}$  commute. The definitions of  $L_v, L_{\text{id}-v}$  in (4.5) yield that this generalized function acts on a test function  $\Phi$  as follows:

$$\langle \tilde{f}(\theta, t), \Phi(\theta) \rangle = e^{-t} \sum_{k=0}^{\infty} \frac{t^k}{k!} \sum_{\gamma \in \Upsilon(k)} \langle \tilde{f}_0(\theta), \Phi \circ \gamma(v, \text{id} - v)(\theta) \rangle,$$

where  $\Upsilon(k) := \{\gamma = (\gamma_1, \dots, \gamma_k) \in \{0, 1\}^k\}$  is the set of all  $k$ -fold permutations and  $\gamma(v_0, v_1) := v_{\gamma_1} \circ \dots \circ v_{\gamma_k}$ .

We will now show that for test function  $\Phi$  on

$$(B.1) \quad \langle \tilde{f}(\theta, t), \Phi(\theta) \rangle \rightarrow \langle \tilde{f}_0(\theta), \theta \rangle \Phi'(0) \quad \text{for } t \rightarrow \infty.$$

Taylor expansion of  $\Phi \circ \gamma(v, \text{id} - v)(\theta)$  in  $\theta = 0$ , and the facts that  $\langle \tilde{f}_0(\theta), 1 \rangle = 0$  and  $\sum_{\gamma \in \Upsilon(k)} \gamma(v, \text{id} - v) = \text{id}$  yield

$$\begin{aligned} &\langle \tilde{f}(\theta, t), \Phi(\theta) \rangle \\ &= \langle \tilde{f}_0(\theta), \theta \rangle \Phi'(0) + e^{-t} \sum_{k=0}^{\infty} \frac{t^k}{k!} \sum_{\gamma \in \Upsilon(k)} \left\langle \tilde{f}_0(\theta), \frac{1}{2} R_\gamma(\theta) \gamma(v, \text{id} - v)(\theta)^2 \right\rangle, \end{aligned}$$

where  $R_\gamma$  is a remainder term with  $\max_{-\pi \leq \theta \leq \pi} |R_\gamma(\theta)| \leq \max_{-\pi \leq \theta \leq \pi} |\Phi''(\theta)|$  for all  $j \geq 0$ .

We want to prove that

$$e^{-t} \sum_{k=0}^{\infty} \frac{t^k}{k!} \sum_{\gamma \in \Upsilon(k)} \left\langle \tilde{f}_0(\theta), \frac{1}{2} R_\gamma(\theta) \gamma(v, \text{id} - v)(\theta)^2 \right\rangle \rightarrow 0 \quad \text{for } t \rightarrow \infty.$$

Because  $|R_\gamma| \leq \max |\Phi''|$  and  $e^{-t} \sum_{k=0}^{\infty} \frac{t^k}{k!} = 1$ , it suffices to show that

$$\sum_{\gamma \in \Upsilon(k)} \gamma(v, \text{id} - v)(\theta)^2 \rightarrow 0 \quad \text{for } k \rightarrow \infty \quad \text{uniformly in } \theta \in [-\pi + \delta, \pi - \delta]$$

for all  $0 < \delta < \pi$ .

Let  $0 < \theta < \pi$  and  $u(\theta) := \max_{0 \leq \psi \leq \theta} \max\{v(\psi), (\text{id} - v)(\psi)\}$ . Because  $v$  is attracting, i.e.,  $0 < v(\theta) < \theta$  and  $0 < (\text{id} - v)(\theta) < \theta$ , it follows that  $0 < u(\theta) < \theta$  and  $(u^k(\theta))_{k \geq 1}$  is monotonically decreasing. Hence  $u^k(\theta) \rightarrow 0$  for  $k \rightarrow \infty$ . The definition of  $u$  implies that  $\gamma(v, \text{id} - v)(\theta) \leq u^k(\theta)$  for any  $\gamma \in \Upsilon(k)$ ; hence,  $\gamma(v, \text{id} - v)(\theta) \rightarrow 0$  for  $k \rightarrow \infty$  uniformly in  $\gamma \in \Upsilon(k)$ . Since  $[0, \pi - \delta]$  is compact, convergence is also uniform in  $\theta$ .

Altogether we have for  $\varepsilon > 0$  fixed and  $k$  large enough

$$0 \sum_{\gamma \in \Upsilon(k)} \gamma(v, \text{id} - v)(\theta)^2 < \varepsilon \sum_{\gamma \in \Upsilon(k)} \gamma(v, \text{id} - v)(\theta) = \varepsilon$$

uniformly in  $\theta \in [0, \pi - \delta]$ , and because  $v$  is odd, convergence holds uniformly on  $[-\pi + \delta, \pi - \delta]$ . This completes the proof of statement (B.1).

**Acknowledgments.** We wish to thank L. Edelstein-Keshet, W. Alt, L. Segel, G. Civelekoglu, and M. Stoll for inspiring ideas, support, and fruitful discussions.

#### REFERENCES

- [1] W. ALT, *Mathematical models in actin-myosin interactions*, in *Nature and Function of Cytoskeletal Proteins in Motility and Transport*, K. E. Wohlfahrt-Bottermann, ed., Gustav Fischer Verlag, Stuttgart, 1987, pp. 219–230.
- [2] G. CIVELEKOGLU AND L. EDELSTEIN-KESHET, *Modelling the dynamics of F-actin in the cell*, *Bull. Math. Biol.*, 56 (1994), pp. 587–616.
- [3] M. DEMBO, F. H. HARLOW, AND W. ALT, *The biophysics of cell surface motility*, in *Cell Surface Dynamics: Concepts and Models*, A. S. Perelson, Ch. deLisi, and F. W. Wiegel, eds., Marcel Dekker, New York, 1983, pp. 495–542.
- [4] L. EDELSTEIN-KESHET AND G. B. ERMENTROUT, *Models for contact-mediated pattern formation*, *J. Math. Biol.*, 29 (1990), pp. 33–58.
- [5] C. W. GARDINER, *Handbook of Stochastic Methods*, Springer-Verlag, Berlin, 1985.
- [6] E. GEIGANT, *Nichtlineare Integro-Differential-Gleichungen zur Modellierung interaktiver Musterbildungsprozesse auf  $S^1$* , Ph.D. thesis, University Bonn., Germany, 1998.
- [7] J. H. HARTWIG, *Mechanisms of actin rearrangements mediating platelet activation*, *J. Cell Biol.*, 117 (1992), pp. 1421–1442.
- [8] E. JÄGER AND L. A. SEGEL, *On the distribution of dominance in populations of social organisms*, *SIAM J. Appl. Math.*, 52 (1992), pp. 1444–1468.
- [9] F. C. MACKINTOSH, J. KÄS, AND P. A. JANMEY, *Elasticity of semiflexible biopolymer networks*, *Phys. Rev. Lett.*, 75 (1995), pp. 4425–4428.
- [10] T. L. MADDEN AND J. HERZFELD, *Crowding-induced organization of cytoskeletal elements*, *Biophys. J.*, 65 (1993), pp. 1147–1154.
- [11] A. I. MOGILNER AND L. EDELSTEIN-KESHET, *Selecting a common direction. I: How orientational order can arise from simple contact responses between interacting cells*, *J. Math. Biol.*, 33 (1995), pp. 619–660.

- [12] A. I. MOGILNER, L. EDELSTEIN-KESHET, AND G. B. ERMENTROUT, *Selecting a common direction. II: Peak-like solutions representing total alignment of cell clusters*, J. Math. Biol., 34 (1996), pp. 811–842.
- [13] A. I. MOGILNER AND L. EDELSTEIN-KESHET, *Spatio-angular order in populations of self-aligning objects: Formation of oriented patches*, Phys. D, 89 (1996), pp. 346–367.
- [14] H. G. OTHMER, S. R. DUNBAR, AND W. ALT, *Models of dispersal in biological systems*, J. Math. Biol., 26 (1988), pp. 263–298.
- [15] B. PFISTNER AND W. ALT, *A two-dimensional random walk model for swarming behaviour*, in Biological Motion, W. Alt and G. Hoffmann, eds., Springer-Verlag, New York, 1989, pp. 564–565.
- [16] T. D. POLLARD AND J. A. COOPER, *Actin and actin-binding proteins: A critical evaluation of mechanisms and functions*, Ann. Rev. Biochem., 55 (1986), pp. 987–1013.
- [17] J. A. SHERRATT AND J. LEWIS, *Stress-induced alignment of actin filaments and the mechanics of cytogel*, Bull. Math. Biol., 55 (1993), pp. 637–654.
- [18] J. V. SMALL, M. HERZOG, AND K. ANDERSON, *Actin filament organization in the fish keratocyte lamellipodium*, J. Cell Biol., 129 (1995), pp. 1275–1286.
- [19] M. STOLL, *private communication*.
- [20] T. P. STOSSEL, *How cells crawl*, Amer. Sci., 78 (1990), pp. 408–423.
- [21] D. H. WACHSSTOCK, W. H. SCHWARTZ, AND T. D. POLLARD, *Cross-linker dynamics determine the mechanical properties of actin gel*, Biophys. J., 66 (1994), pp. 801–809.
- [22] V. ZHUKAREV, F. ASHTON, J. M. SANGER, J. W. SANGER, AND H. SHUMAN, *Organization and structure of actin filament bundles in Listeria-infected cells*, Cell Motil. Cytoskeleton, 30 (1995), pp. 229–246.